HYPERSPECTRAL VERSUS MULTISPECTRAL SATELLITE DATA FOR URBAN LAND COVER AND LAND USE MAPPING — BEIJING, AN EVOLVING CITY

Qiyun Tan, MSc Candidate
Jinfei Wang, Professor
Department of Geography
University of Western Ontario
London, ON N6A 5C2
qtan@uwo.ca
jfwang@uwo.ca

ABSTRACT

Beijing is currently experiencing rapid land cover and land use (LCLU) changes. Monitoring such changes is necessary since the change information will help to manage land effectively. Remote sensing technique provides timely and accurate information of land cover and land use in urban areas. The objective of this research is to evaluate the feasibility of hyperspectral satellite imagery for urban LCLU mapping and compare the performance of multispectral and hyperspectral data in urban studies. A Chris-Proba image of northern part of Beijing collected from a hyperspectral satellite and an ASTER image collected from a multispectral satellite were analyzed and compared. The results show that hyperspectral satellite imagery is suitable for urban LCLU mapping. In addition, it is demonstrated that the hyperspectral satellite image provides more accurate classification results than those extracted from the multispectral satellite image in urban LCLU mapping.

INTRODUCTION

Information about land cover and land use concerns many groups of people like local governors, land managers, urban planners and decision makers, especially those in the urban areas which are undergoing dramatic land cover and land use changes, such as Beijing, China. They need to keep track of the situation of land cover and land use, and record the information in a timely and accurate manner, in order to update the database of urban land cover and land use frequently to manage land and plan land use efficiently and make relative decisions judgmatically. Hence, they are interested in effective methods for land cover and land use mapping (Roessner et al., 2001).

A series of impressive developments achieved in recent years on remote sensing analytical techniques, as well as increasing availability and improved quality of remotely sensed data, have demonstrated that remote sensing technique can probably offer accurate, cost-effective, and timely geospatial information for land cover and land use classification (Yang, 2002; Yang et al., 2003; Zhang et al., 2001).

Since one of the most important characteristics of urban areas is the extremely dense and various use of space, the accurate detection of land cover and land use classes in the complex urban environment using satellite remote sensing is a challenging task.

Multispectral data have been widely applied in urban studies for land cover and land use mapping (Xu and Gong, in press). As commonly used and low-cost multispectral satellite imagery, Advanced Spaceborne Thermal Emission and Reflection Radiometer (ASTER) imagery has been used to classify land cover and land use types accurately in the urban environment but with fewer classes (Zhu and Blumberg, 2002).

On the other hand, hyperspectral satellite imagery is considered as a valuable data source for land cover and land use mapping. Hyperspectral imagery contains detailed land usage information collected simultaneously from hundreds of narrow bands (Lillesand and Kiefer, 2000). These bands are so sensitive to ground features that it is possible to record detailed information about earth surface. In addition, materials which have similar spectral features are possible to be discriminated (Lillesand and Kiefer, 2000). However, to date, there is little research working on hyperspectral satellite data for urban land cover and land use mapping. As a result, accurate classification results with various land cover and land use classes are expected to be derived from a hyperspectral satellite image.

This study focuses on the classification of multispectral and hyperspectral satellite imagery, in order to: (1) test the potential of hyperspectral satellite data for urban land cover and land use mapping; and (2) evaluate the urban mapping performance of multispectral and hyperspectral satellite images.

STUDY AREA AND DATA DESCRIPTION

The study area is located in Beijing, the capital city of China. Land cover and land use structures are complicated in Beijing, and different parts of the city have different patterns of land cover and land use (Cao, 2002; Niu and Ding, 2006). Moreover, the city is growing at a fast pace because of the flourishing economy and the large population.

In this research, two images were aquired. One is a multispectral image, ASTER. It was collected by Advanced Spaceborne Thermal Emission and Reflection Radiometer instrument aboard Terra, a satellite launched in December 1999 by National Aeronautics and Space Administration (NASA). This data set (Figure 2) was recorded on April 22, 2006 with 15 bands from three telescopes: (1) 4 bands in visible and near infrared (VNIR) with 15m spatial resolution; (2) 6 bands in short wave infrared (SWIR) with 30m spatial resolution; and (3) 5 bands in thermal infrared (TIR) with 90m spatial resolution. Moreover, it is a Level-1B product from the Land Processes DAAC company, which implies that the radiometric calibration and geometric correction coefficients have been applied.

The other image is a hyperspectral image. It was collected by Compact High Resolution Imaging Spectrometer (Chris) sensor which is carried on Project for On Board Autonomy (Proba), a satellite launched on October 22, 2001 by European Space Agency. The instrument provides several modes which have their own specific goals. For example, mode 2 is for water studies while mode 3 is for land studies. The image was recorded on September 17, 2005 by mode 3 over north part of Beijing. It contains 18 bands that cover a wavelength range from 438 to 1035 nanometers （Table 1）. For the given data, Chris instrument flied at an altitude of 556km, providing 17m spatial resolution at nadir. (Figure 1 shows the false color composite of the Chris-Proba image.) Since the wavelength ranges of the first three bands of the ASTER image correspond to that of the 18 bands of the Chris-Proba image (Table 1) and the three bands have similar spatial resolution as that of the Chris-Proba image, the first three ASTER bands were selected for the classification.

Table 1. Left: Wavelength ranges of the ASTER image. Right: Wavelength ranges of the Chris-Proba image.

ASTER Bands	Wavelength (μm)
1	0.52 - 0.60
2	0.63 – 0.69
3 (nadir)	0.76 – 0.86

Chris-Proba Bands	Wavelength (μm)	Chris-Proba Bands	Wavelength (μm)	Chris-Proba Bands	Wavelength (μm)
1	0.438-0.447	7	0.656-0.666	13	0.745-0.752
2	0.486-0.495	8	0.666-0.677	14	0.773-0.788
3	0.526-0.534	9	0.694-0.700	15	0.863-0.881
4	0.546-0.556	10	0.700-0.706	16	0.891-0.900
5	0.566-0.573	11	0.706-0.712	17	0.900-0.910
6	0.627-0.636	12	0.738-0.745	18	0.1002-0.1035

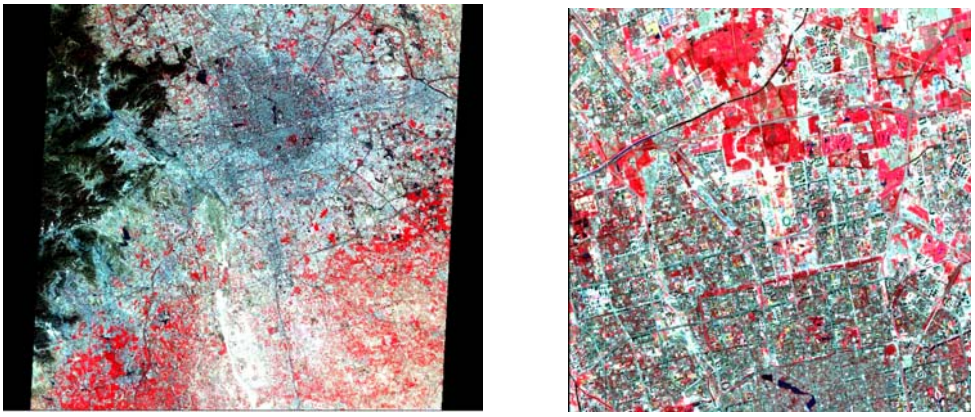

Figure 1. Left: ASTER image covering Beijing, recorded on April 22, 2006 (bands 3, 2, 1 as RGB). Right: Chris-Proba image covering north Beijing, collected on September 17, 2005 (bands 16, 8, 4 as RGB).

Beijing is a city possessing multiple ring roads. From the two images, it can be seen that the second, the third, the fourth and the fifth ring roads as part of the road network. In terms of buildings, most of the high-rise buildings were built in the last decade and can be considered as high density buildings. Furthermore, most of the low-rise buildings, especially those ones within the second ring road, were built a long time ago and can be regarded as s. Moreover, vegetation areas with regular shapes, like rectangles, are agriculture areas while those with irregular shapes, along road networks or around buildings are probably covered by trees or grass.

METHODOLOGY

Preprocessing

In this study, bands 1, 2 and 3 of the ASTER image were geometrically corrected with 60 ground control points (GCPs) provided by the LP DAAC company. The RMS is 0.03 with a third polynomial order.

The geometric correction of the ASTER image was followed by image subsetting. A study subscene of 700 x 760 pixels covering the same ground area as the Chris-Proba image was selected from bands 1, 2 and 3 for comparison purpose (Figure 2).

Figure 2. A subscene of the geometrically corrected ASTER image over the study area (bands 3, 2 and 1 as RGB).

One difficulty with using the Chris-Proba image is that it contains some noise such as stripes. Among all 18 bands in the Beijing image, there are hundreds of tiny vertical stripes, especially an obvious vertical stripe shown in the west part of the image. In order to remove the stripes with minimum influence in the whole image, destriping function was applied to the 18 bands with window size of 7. Figure 3 presents the results of destriping function. The

top left image is a subscene of band 2 before destriping and the top right one is the subscene after destriping; the bottom left one shows a subscene of the false color composite showing the obvious vertical stripe while the bottom right one is the subscene after destriping. It can be seen that the stripes were removed after applying destriping function.

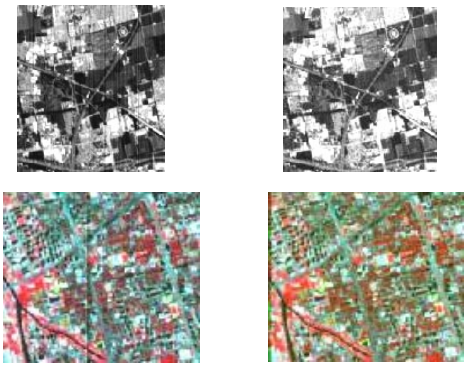

Figure 3. The results of destriping function.

The Chris-Proba image was geometrically corrected to the registered ASTER image using a fourth order polynomial. 60 GCPs were used with X, Y RMS errors of 0.33 and 0.36 pixels. The image was resampled into 15m spatial resolution and projected in UTM coordinate system as well. A subscene of 700 x 760 pixels covering the same part of north Beijing as that of the ASTER image was selected from original Chris-Proba image for the research (Figure 4).

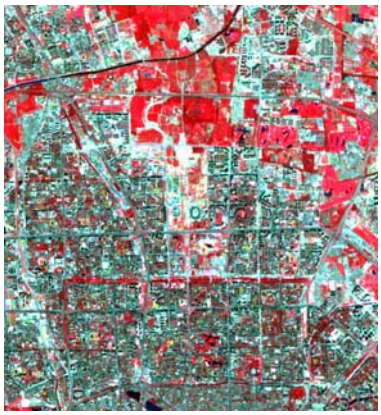

Figure 4. A subscene of the Chris-Proba image after preprocessing.

In order to reduce the dimensionality of the hyperspectral dataset, principal components analysis (PCA) was applied to the geometrically corrected Chris-Proba image. The first four components generated by using PCA function account for 99.79% of the variance in the entire dataset while the fifth component accounts for 0.19% of the remaining variance. Therefore, the first four principal components including most of the variance were used in the classification.

Classification

In this study, the U.S. Geological Survey Land Use/Land Cover Classification System was adopted for both images as classification system. The classes are Grass, Trees, Roads, Bare Soil, Agriculture, High Density Buildings, s, Water and Other Built-up areas. Maximum Likelihood classification approach was applied to the ASTER image (band 1, 2 and 3) and the Chris-Proba image (PC1 to PC4) respectively. Training sites were collected based on field data collected in 2005, Beijing atlases and Beijing maps. Initially, training sites were chosen for 18 sub-classes derived from the ASTER image and 29 sub-classes derived from the Chris-Proba image. As for the ASTER image, 18 sub-classes were aggregated into the nine proposed classes while for the Chris-Proba image, 29 sub-classes were

aggregated into the nine proposed classes too. 200 testing points were generated randomly for each of the two images for accuracy assessment.

RESULTS AND DISCUSSION

In this project, both the ASTER and the Chris-Proba images were classified into nine land cover and land use classes. Figure 5 shows the resultant maps of classification of the ASTER and the Chris-Proba images.

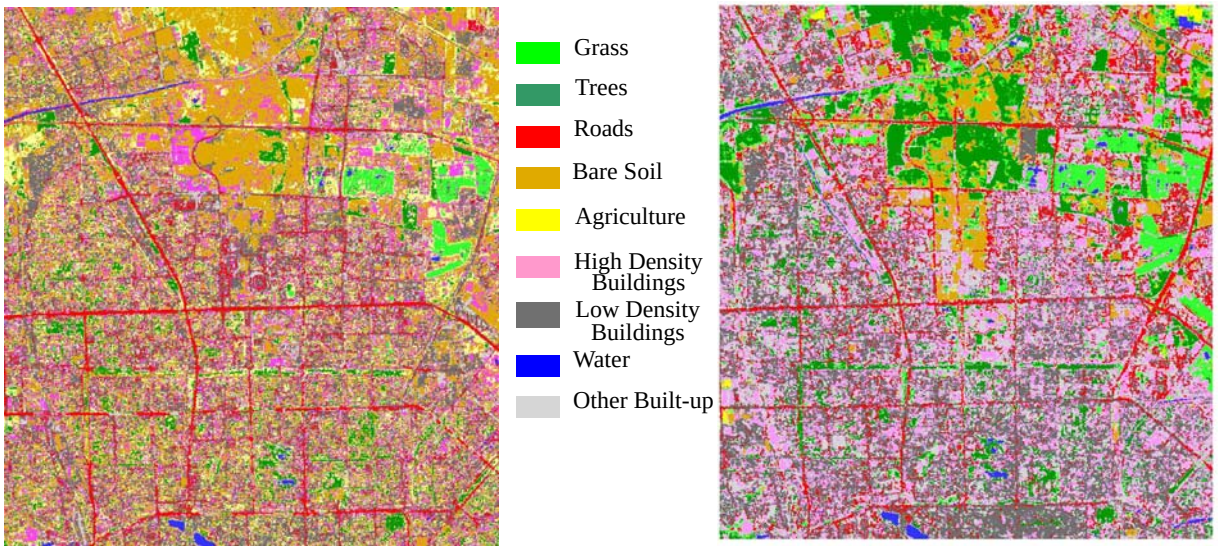

Figure 5. Left: Classification result derived from the ASTER image.
Right: Classification result derived from the Chris-Proba image.

The overall accuracy and kappa coefficients of the classification results derived from the ASTER and the Chris-Proba images are shown in Table 2. The producer's and user's accuracies of both images are shown in Table 3.

From the results, the Chris-Proba image produces a higher overall accuracy and kappa than that of the ASTER image. The comparison between overall accuracy and kappa concerning the data types indicates that the Chris-Proba provides a better discrimination among different land cover and land use types while the ASTER yields less satisfactory result.

Table 2. Comparison of overall accuracy and kappa for the ASTER and Chris-Proba images.

Images	Overall Accuracy	Kappa
ASTER	82%	0.78
Chris-Proba	88%	0.86

Table 3. Left: Producer's and user's accuracies of the ASTER image.
Right: Producer's and user's accuracies of the Chris-Proba image.

ASTER Classes	Producer's Accuracy	User's Accuracy
Grass	100%	100%
Trees	73%	100%
Roads	79%	85%
Bare Soil	90%	70%
Agriculture	100%	67%
High Density Buildings	58%	88%
Low Density Buildings	89%	98%
Water	100%	100%
Other Built-up	85%	73%

Chris-Proba Classes	Producer's Accuracy	User's Accuracy
Grass	100%	94%
Trees	75%	100%
Roads	100%	58%
Bare Soil	100%	100%
Agriculture	100%	100%
High Density Buildings	85%	95%
Low Density Buildings	83%	100%
Water	100%	100%
Other Built-up	100%	77%

For the ASTER image, both producer's accuracy and user's accuracy above 80% can be achieved in the classes of Grass, Low Density Buildings and Water. On the other hand, Grass, Bare Soil, Agriculture, High Density Buildings, Low Density Buildings, Water were well classified into correct classes in the Chris-Proba image since both producer's and user's accuracies are above 80%.

Meanwhile, the class of High Density Buildings shows the lowest producer's accuracy of 58% in ASTER image, which is much lower than the one from the Chris-Proba image. This is mainly because the bands of the Chris-Proba are narrow enough to record feature information at a fine level and distinguish rooftops with different materials, which can be proved by the spectral curves of High Density Buildings. The curves extracted from the Chris-Proba are separated while those of the ASTER image are overlapped.

Moreover, the lowest user's accuracy of 67% in ASTER image is observed in the class of Agriculture, which is confused with the class of Trees. This occurs due to the same or similar spectral signature. From the spectral curves, part of curve of Agriculture is overlapped with that of coniferous trees and deciduous trees, which supports the argument that they are indistinguishable because of the limitation of wavelength ranges.

In the classification results of the Chris-Proba image, the class of Trees obtains the lowest producer's accuracy of 75% while the class of Roads has the lowest user' accuracy of 58%. These are not because of the spectral resolution, but mainly because of the medium spatial resolution of the image. With 15m resolution, narrow roads are difficult to be distinguished from trees beside the roads.

CONCLUSIONS

Remote sensing technique provides proper tools to record timely and accurate information of land cover and land use. This study focuses on the classification of multispectral and hyperspectral satellite images for land cover and land use in complex urban environment. Nine classes of land cover and land use are derived from the ASTER image and the Chris-Proba image. They are Grass, Trees, Roads, Bare Soil, Agriculture, High Density Buildings, Low Density Buildings, Water and Other Built-up. The overall accuracy of Chris-Proba classification is 88% with overall kappa of 0.86. The overall accuracy of ASTER classification is 82% with overall kappa of 0.78.

This paper demonstrated that the Chris-Proba image is preferred in urban land cover and land use mapping in the study area, since both the overall accuracy and kappa are higher than those of the ASTER image. In addition, this research confirms that the Chris-Proba image contains more details than the ASTER image at a fine level and enables us to distinguish features with similar spectral signatures which are indistinguishable using multispectral remotely sensed data.

ACKNOWLEDGEMENTS

The authors would like to thank the European Space Agency for providing the Chris-Proba data and technical support. This research is funded by a Natural Science and Engineering Research Council of Canada granted to Dr. Jinfei Wang.

REFERENCES

Cao, J. (2002). *China City Land Efficient Use Research.* Economics Management Inc., Beijing, pp. 117-141.

Lillesand, T., and R. Kiefer (2000). *Remote Sensing and Image Interpretation.* John Wiley & Sons, Inc., New York, pp. 363-370.

Liu, J. G. (2000). Smoothing filter-based intensity modulation: a spectral preserve image fusion technique for improving spatial details. *International Journal of Remote Sensing,* 21(18): 3461-3472.

Niu, L., and G. Ding (2006). Study on Sustainable Use of Soil Resources in Beijing. *Research of Soil and Water Conservation,* 13(5): 175-179.

Roessner, S., K. Segl, U. Heiden, and H. Kaufmann (2001). Automated Differentiation of Urban Surfaces Based on Airborne Hyperspectral Imagery. *GEOSCIENCE AND REMOTE SENSING*, 39(7): 1525-1532.

Xu, B., and P. Gong (In press). Land use/cover classification with multispectral and hyperspectral EO-1 data: a comparison. *Photogrammetric Engineering & Remote Sensing.*

Yang, L., G. Xian, J. Klaver, and B. Deal (2003). Urban Land - Cover Change Detection through Sub – Pixel Imperviousness Mapping Using Remotely Sensed Data. *Photogrammetric Engineering & Remote Sensing,* 69(9): 1003-1010.

Yang, X. (2002). Satellite monitoring of urban spatial growth in the Atlanta metropolitan area. *Photogrammetric Engineering and Remote Sensing,* 68(7): 725-734.

Zhang, Q., J. Wang, X. Peng, P. Gong, and P. Shi (2001). Urban built-up land change detection with road density and spectral information from multi-temporal Landsat TM data. *International Journal of Remote Sensing,* 23(15): 3057-3078.

Zhu, G., and D. G. Blumberg (2002). Classification using ASTER data and SVM algorithms;-The case study of Beer Sheva, Israel. *Remote Sensing of Environment,* 80(2): 233-240.